

Design and Electrochemical Performance of Ni-MOF/rGO Heterostructures for High-Capacity Supercapattery

Mayank K. Singh, Sheetal Gupta, Khushwant Singh, Suporna Bhowmick, Govind Kumar Maurya, and Dharendra K. Rai*

Sustainable Energy and Environmental Materials (SEEM) Lab, Department of Metallurgical Engineering and Materials Science, Indian Institute of Technology Indore, Simrol, Indore 453552, India.

*Corresponding author: Dr. Dharendra K. Rai, E-mail: dkrai@iiti.ac.in; Tel: +91 731 660 3278

List of Content

- 1) Chemicals
- 2) Preparation of electrode and electrochemical testing
- 3) Physicochemical Characterization
- 4) Three electrode measurement
- 5) Solid-state device fabrication
- 6) Synthesis of Reduced Graphene Oxide
- 7) Synthesis of rGO
- 8) **Figure S1.** TGA Ni-MOF and rGO.
- 9) **Figure S2(a,b).** FTIR of Ni-MOF and rGO.
- 10) **Figure S3.** N₂ adsorption-desorption curve of Ni-MOF and rGO.
- 11) **Figure S4.** Raman Spectra of Ni-MOF, rGO and Ni-MOF/rGO.
- 12) **Figure S5 (a).** Full survey XPS spectra of Ni-MOF/rGO **(b)** XPS spectra of Ni 2p **(c)** XPS spectra of C 1s **(d)** XPS spectra of N 1s **(e)** XPS spectra of O 1s
- 13) **Figure S6.** Optimization of potential range of Ni-MOF/rGO electrode (a,b) CV in positive and negative range (c,d) GCD in positive and negative range.
- 14) **Figure S7.** Cyclic Voltammetry of Ni-Foam compared with Ni-MOF/rGO composite.
- 15) **Figure S8 (a,b,c).** Charge storage kinetics using power law for Ni-MOF, rGO and Ni-MOF/rGO composite respectively.
- 16) **Figure S9. (a,b)** Dunn's analysis at different scan rates.
- 17) **Figure S10.** GCD of Ni-MOF and rGO at different current densities.

18) **Figure S11.** EIS Circuit of (a) Ni-MOF (b) rGO and (d) Ni-MOF/rGO.

19) **Table S1.** Comparison table of different Ni-MOFs and their derivatives with Ni-MOF/rGO.

20) **Table S2.** The fitted parameter values for EIS data of Ni-MOF, rGO and Ni-MOF/rGO.

21) **Figure S12.** Stability study of Ni-MOF/rGO till 5000 cycles.

22) **Figure S8a.** FE-SEM of Ni-MOF/rGO after 5000 cycles.

1. Chemicals

Graphite flakes with a purity of 99.5%, sodium nitrate (NaNO_3) at 98% purity, potassium permanganate (KMnO_4) at 99.0% purity, hydrogen peroxide (H_2O_2) at 50% concentration, and hydrochloric acid (HCl) at 35% concentration were purchased from chemical suppliers SRL and TCI. For this experiment, nickel nitrate hexahydrate ($\text{Ni}(\text{NO}_3)_2 \cdot 6\text{H}_2\text{O}$) with 98% purity, 2-methylimidazole, and methanol were obtained from local commercial sources and used as it is. Ethanol was sourced from Changshu Hongsheng supplier. Deionized water with a resistivity of 18.2 $\text{M}\Omega \text{ cm}$ was used in all experiments that involved water.

2. Preparation of electrode and electrochemical testing

To prepare three functional electrodes, the as-synthesized Ni-MOF, rGO, and Ni-MOF/rGO were coated on separate Ni-Foams, serving as the current collectors. Three slurries were prepared by mixing 20 mg of each material in 2 mL of ethanol (10 mg mL^{-1} concentration) in separate vials, followed by ultrasonication to ensure proper dispersion of the materials. Subsequently, 100 μL of each slurry was uniformly coated onto the carbon paper current collectors.

3. Physicochemical Characterization

Crystallinity and phase investigations were conducted using powder X-ray diffraction (PXRD) with Bruker's AXA D8 Advance equipment. The measurements were taken at a scanning rate of 0.02° per minute within the 2θ range of 10° to 80° , using $\text{CuK}\alpha$ radiation ($\lambda = 1.54 \text{ \AA}$) as the source. Thermogravimetric analyses were performed using a gravimetric analyzer from Mettler Toledo at a heating rate of 10°C per minute, ranging from ambient temperature to 800°C , to assess the thermal characteristics and stability of the sample. Fourier-transform infrared (FTIR) spectra were acquired using a Bruker Tensor 27 spectrometer, recorded across a wavelength range of 400 to 3000 cm^{-1} . Additionally, the morphology and elemental composition of the

sample were analyzed using a Field Emission Scanning Electron Microscope (FESEM) (JEOL-7610F Plus), which was equipped with Energy Dispersive Spectroscopy (EDS).

4. Three electrode measurement

All electrochemical tests were conducted using an Autolab PGSTAT 204N, controlled by NOVA software (version 1.10), under ambient conditions. The experiments were conducted in a three-electrode setup, with Ag/AgCl as the reference electrode, platinum as the counter electrode, and Ni-Foam coated with the active material serving as the working electrode. Cyclic voltammetry (CV) and galvanostatic charge-discharge (GCD) tests were performed across a potential window of 0 to 0.6 V, with varying scan rates and current densities. Electrochemical impedance spectroscopy (EIS) was conducted over a frequency range from 10 mHz to 100 kHz, applying a 10 mV AC signal.

The specific capacities were calculated from the discharge curves of the GCD tests using the following equation.

$$C = \frac{I \Delta t}{m} \quad (1)$$

Where C is the specific capacity (Cg^{-1}), I is current (A), Δt is the discharge time (s), and m is the mass of the coated active material (g).

5. Solid-state device fabrication

The solid-state symmetrical charge storage device was fabricated using a Swagelok cell having a 16 mm diameter. The slurry of electrode materials for device fabrication was prepared by mixing 80% active materials, 10% carbon black, and 10% polyvinylidene difluoride (PVDF) in a few drops of N-methyl pyrrolidone (NMP). Thereafter, the as-obtained slurry was coated on a clean 13 mm diameter circular Ni-Foam and dried in an oven for 8 h at 60°C. The electrolyte solution was prepared by adding 1g of PVA in 10 mL of water; subsequently, the resultant solution was heated at 90°C for 3 h with continuous stirring, followed by adding 10 mL of 1M KOH solution. Afterward, both electrodes were dipped in the polyvinyl alcohol-potassium hydroxide (PVA-KOH) electrolyte and partially dried in an oven. Finally, the device was fabricated by sandwiching a cellulose paper separator with two Ni-foam circular cuttings coated with electrode materials. The fabricated device's specific capacity (C), energy density (E), and power density (P) were calculated from the GCD curves using the following equations.

$$C = \frac{2I \Delta t}{m} \quad (2)$$

$$E \left(\frac{Wh}{kg} \right) = \frac{0.5 \times C \Delta V}{3.6} \quad (3)$$

$$P \left(\frac{W}{kg} \right) = \frac{3600 \times E}{\Delta t} \quad (4)$$

Where C is the specific capacity (C.g-1), I is current (A), Δt is the discharge time (s), m is the combined mass of the coated active material on both electrodes (g), and ΔV is the potential range.

6. Synthesis of Reduced Graphene Oxide

The syntheses of reduced graphene oxide were done using chemical reduction of graphene oxide (GO). For the reduction of GO to obtain rGO, 100 mg of GO was dispersed in 10 mL DI water. To this dispersion, a solution of 1g of NaBH_4 in 6 mL DI water was added gradually, and the resulting mixture was refluxed for 24 h. Afterward, the product was filtered and washed thoroughly with DI water and ethanol and dried in a vacuum oven.

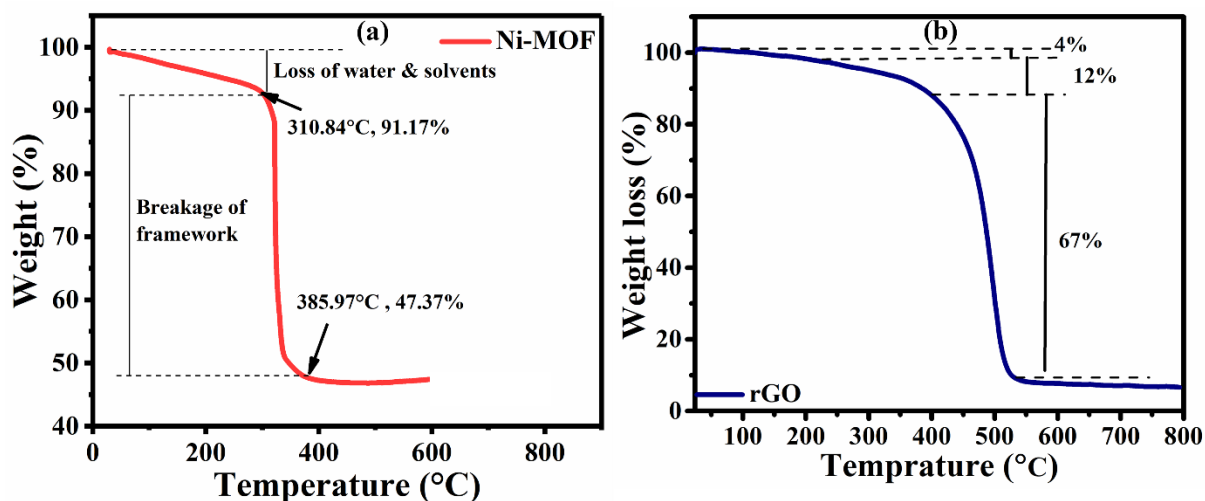


Figure S1(a,b). TGA profiles of Ni-MOF and rGO.

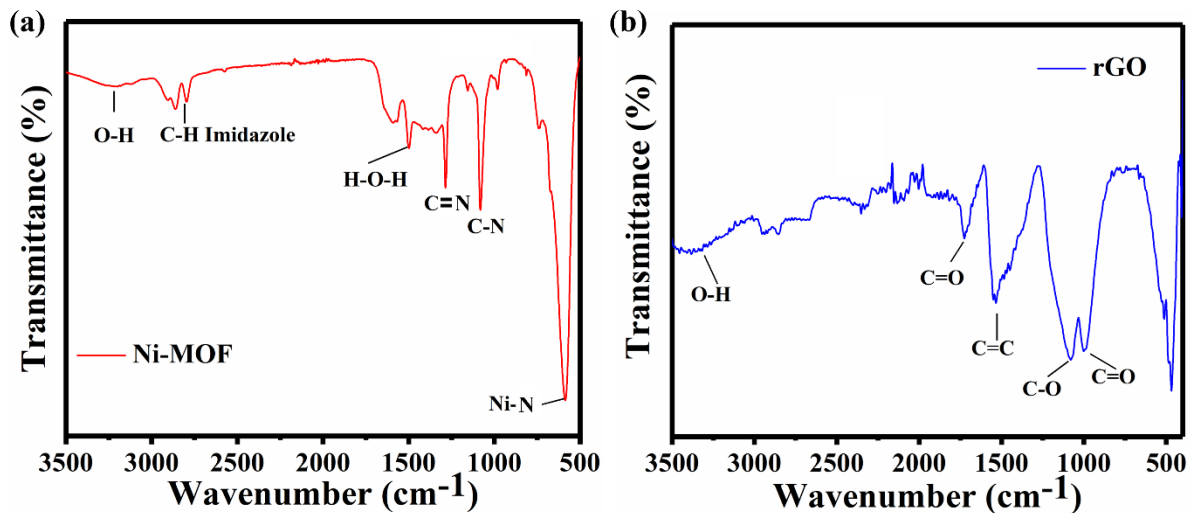


Figure S2(a,b). FTIR of Ni-MOF and rGO.

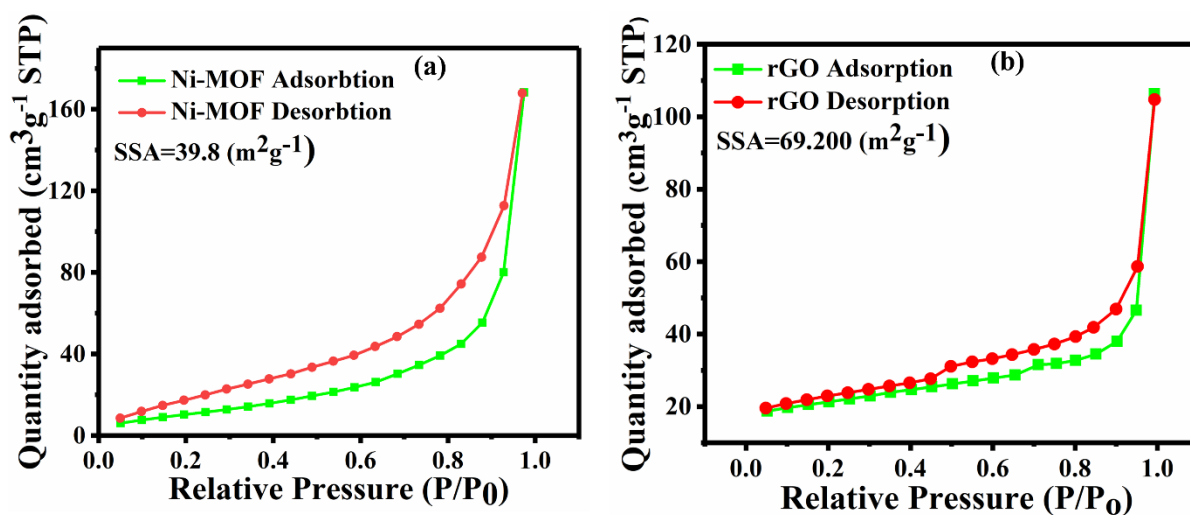


Figure S3 (a,b). N_2 adsorption-desorption curve of Ni-MOF and rGO.

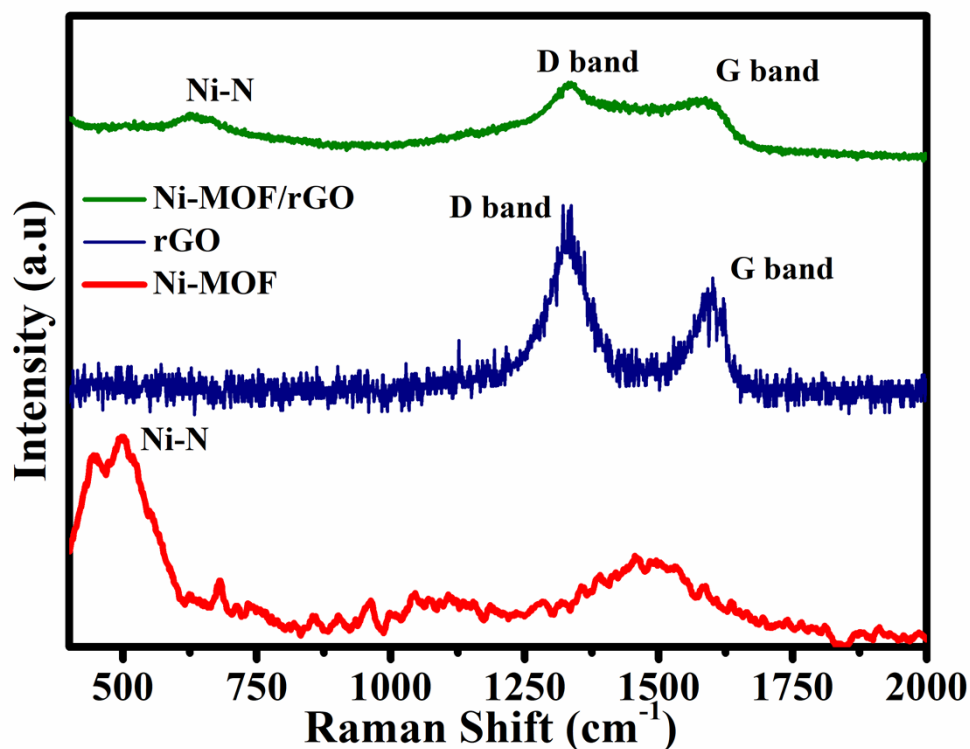


Figure S4. Raman Spectra of Ni-MOF, rGO, and Ni-MOF/rGO.

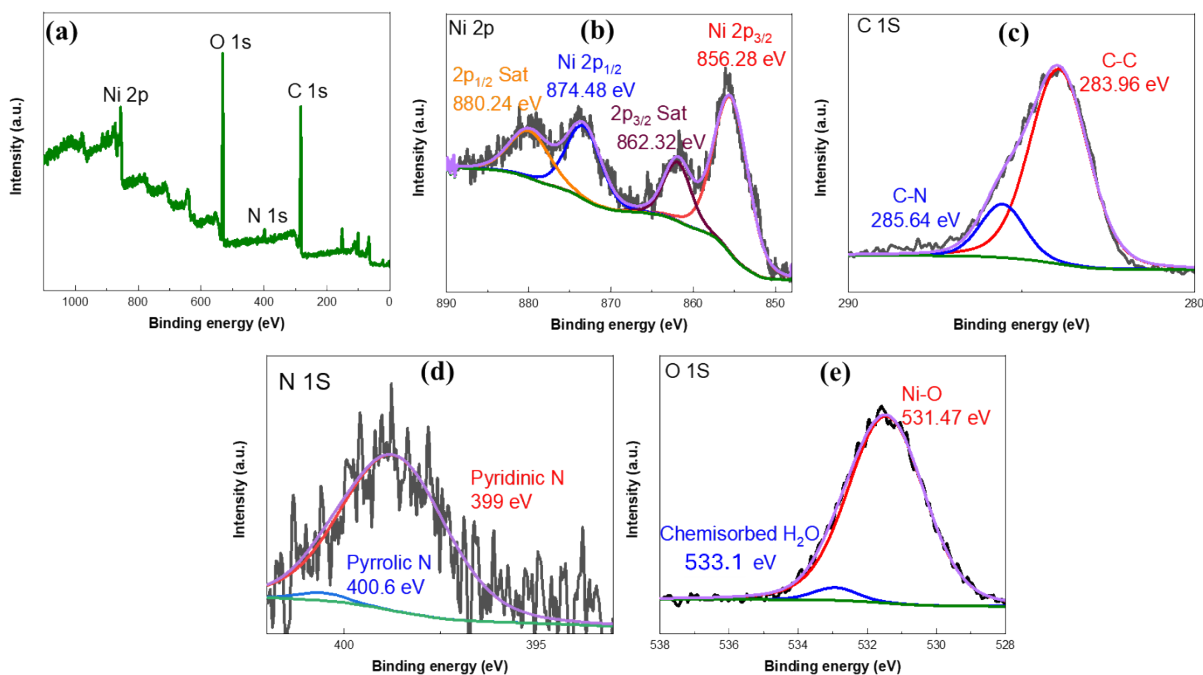


Figure S5 (a). Full survey XPS spectra of Ni-MOF/rGO (b) XPS spectra of Ni 2p (c) XPS spectra of C 1s (d) XPS spectra of N 1s (e) XPS spectra of O 1s

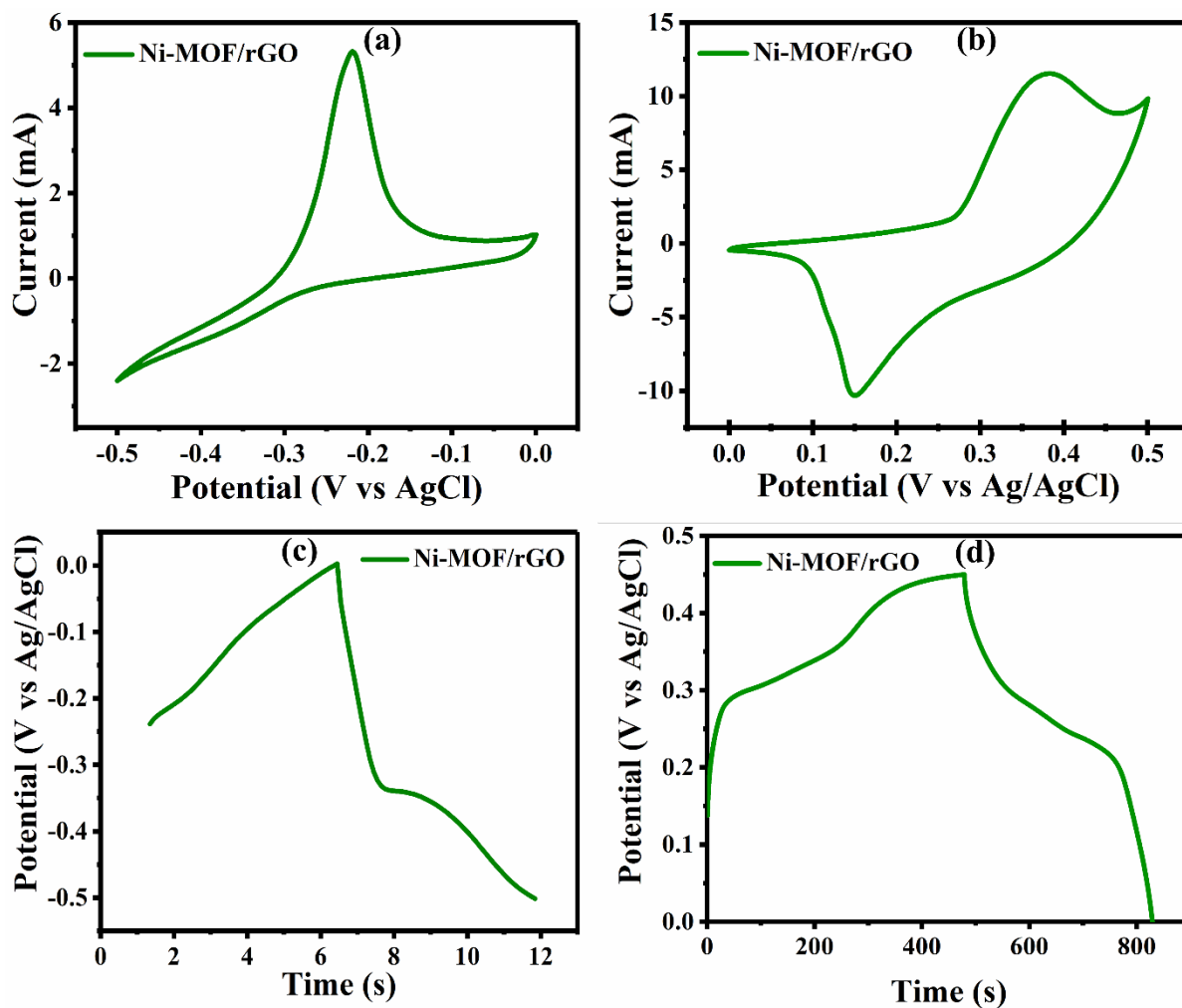


Figure S6(a-d). Optimization of potential range for Ni-MOF/rGO electrode (a,b) CV in positive and negative range (c,d) GCD in positive and negative range.

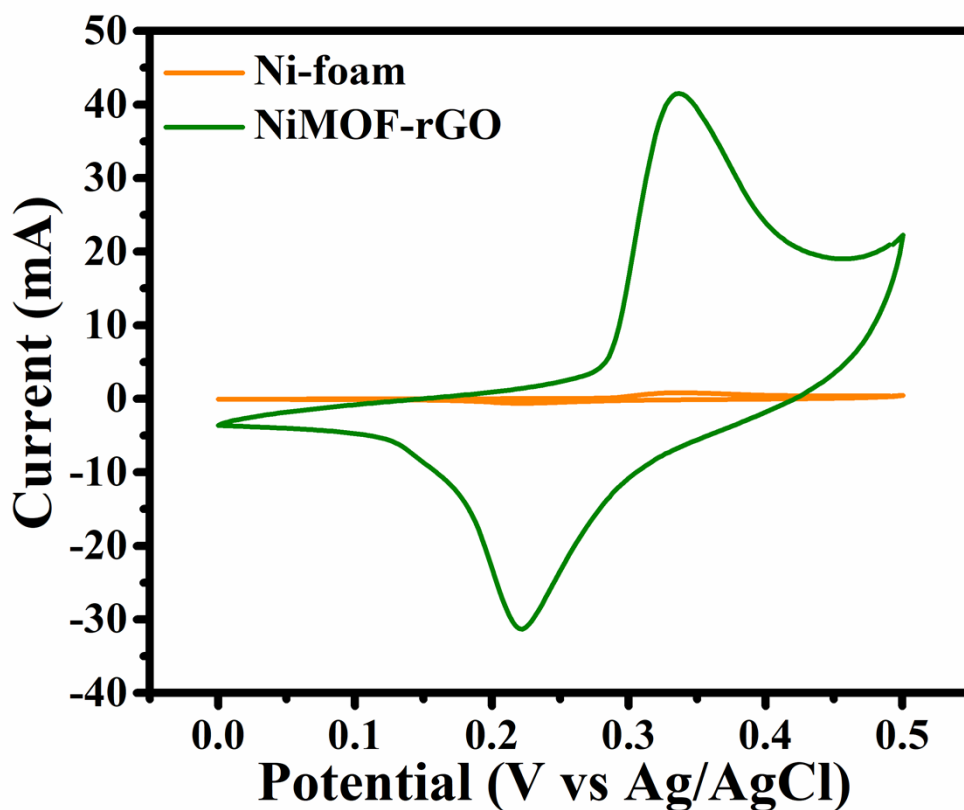


Figure S7. Cyclic Voltammetry of Ni-Foam compared with Ni-MOF/rGO composite.

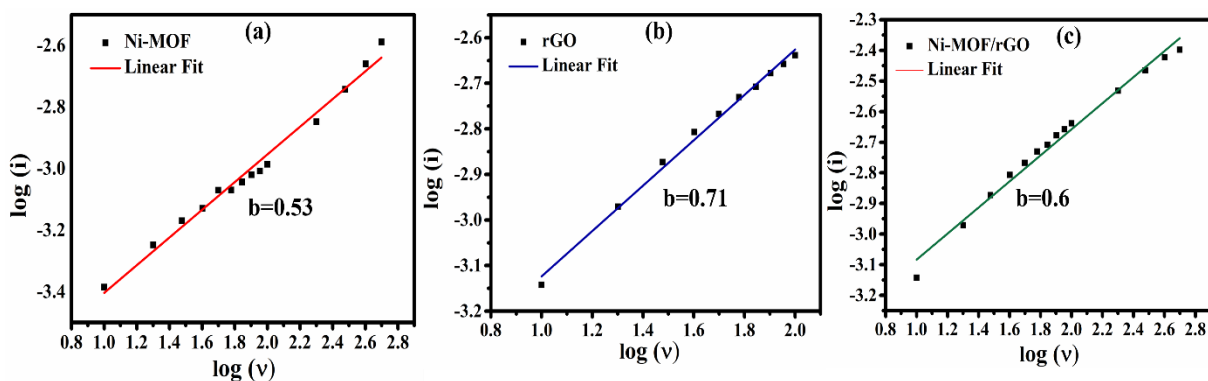


Figure S8 (a,b,c). Charge storage kinetics using power law for Ni-MOF, rGO and Ni-MOF/rGO composite respectively.

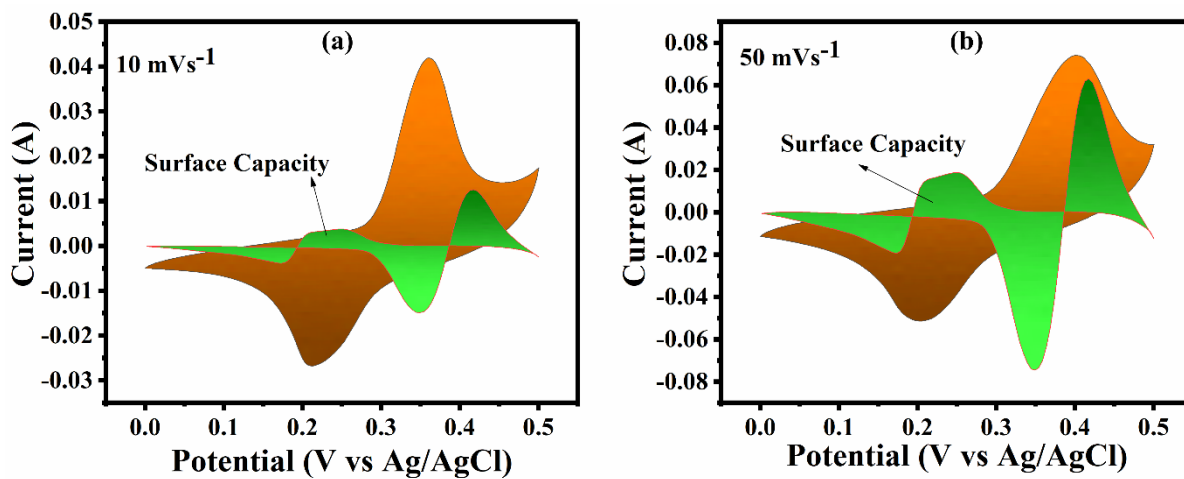


Figure S9. (a,b) Proportion of cyclic voltammogram arising from surface-controlled process to the overall voltammogram of Ni-MOF/rGO at 10 and 50 mV/sec.

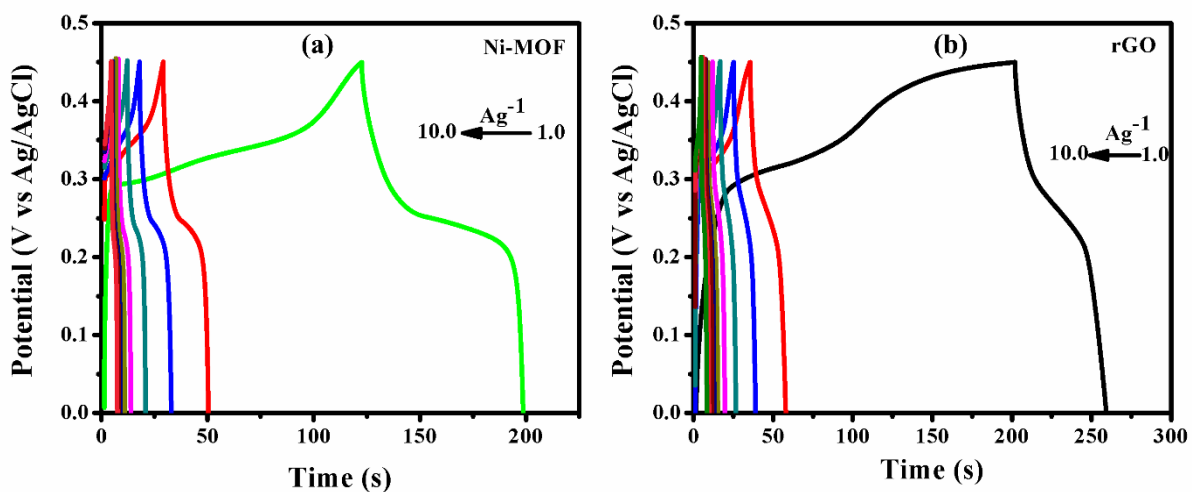


Figure S10 (a,b). GCD of Ni-MOF and rGO at different current densities.

Table S1. Comparison table of different Ni-MOFs and their derivatives with Ni-MOF/rGO.

Electrode	Electrolytes	Current density	Specific capacitance /capacity	References
Ni-MOF/rGO	6M KOH	1 Ag ⁻¹	435.25 Fg ⁻¹	1
rGO/Ni-MOF/PANI	1M H ₂ SO ₄	0.2 Ag ⁻¹	195.14 Fg ⁻¹	2
Ni-MOF@PPy	2M KOH	0.5 Ag ⁻¹	1815.4 F g ⁻¹	3
Ni-MOF/MWCNT	1M H ₂ SO ₄	0.5 Ag ⁻¹	900 F g ⁻¹	4
Ni-MOF@CNF	6M KOH	1 Ag ⁻¹	742.2F g ⁻¹	5
Ni-MOF/rGO	1M KOH	1 A/g	349 Cg ⁻¹ /698Fg ⁻¹	This study

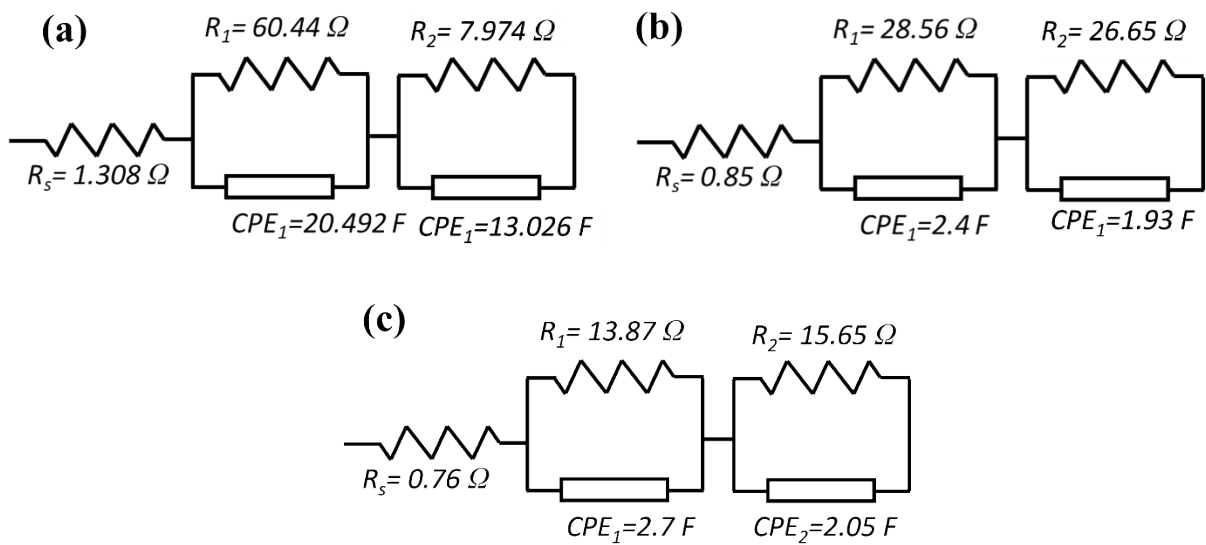


Figure S11. EIS Circuit of (a) Ni-MOF (b) rGO and (d) Ni-MOF/rGO.

Table S2. The fitted parameter values for EIS data of Ni-MOF, rGO and Ni-MOF/rGO.

S.N.	Parameter	Ni-MOF	rGO	Ni-MOF/rGO
1.	R_s (m Ω)	1.308	0.85	0.76
2.	R_{ct} (m Ω) or R_1	60.44	28.56	13.87
3.	R_2 (m Ω)	7.974	26.65	115.65
4.	CPE (mMho)	20.492	2.4	2.7
5.	CPE (mMho)	13.026	1.93	2.05

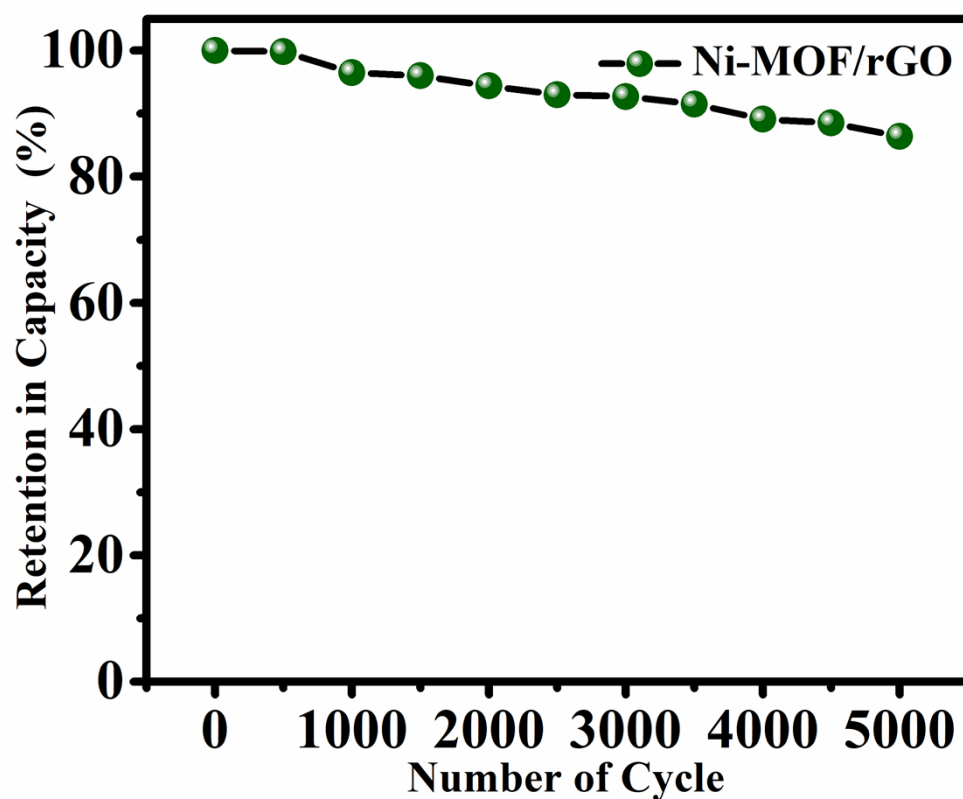


Figure S12. Stability study of Ni-MOF/rGO till 5000 cycles.

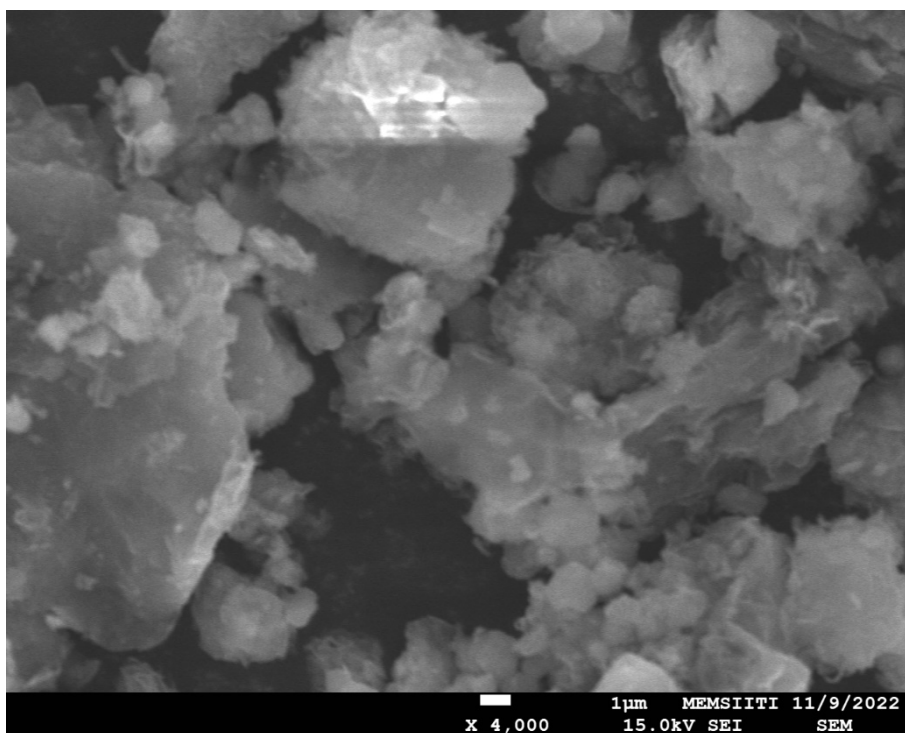


Figure S13. FE-SEM of Ni-MOF/rGO after 5000 cycles.

References

- 1 X. Li, J. Li, Y. Zhang and P. Zhao, *Colloids and Surfaces A: Physicochemical and Engineering Aspects*, 2021, **622**, 126653.
- 2 Q. B. Le, H. Fei, C. Bubulinca, F. A. Ngwabebhoh, N. E. Kazantseva and P. Saha, *ECS Trans.*, 2020, **99**, 93–101.
- 3 Z. Qin, Y. Xu, L. Liu, M. Liu, H. Zhou, L. Xiao, Y. Cao and C. Chen, *RSC Adv.*, 2022, **12**, 29177–29186.
- 4 S. Yazdani, M. S. Lashkenari and F. Mehri, *Synthetic Metals*, 2024, **307**, 117702.
- 5 S. Shin and M. W. Shin, *Applied Surface Science*, 2021, **540**, 148295.